Receiver Function Derived Structural Constraints on Dynamic Proccesses Associated with the Young Nazca Lithosphere Subducting beneath Colombia

Brandon T. Bishop,[*1] Sungwon Cho,[1] Linda M. Warren,[1] Patricia Pedraza García,[2] Germán A. Prieto,[3] Viviana Dionicio[2]

*email: brandon.t.bishop@slu.edu [1]Department of Earth & Atmospheric Sciences, Saint Louis University, St. Louis, MO, USA;[2]Red Sismológica Nacional de Colombia, Servicio Geológico Colombiano, Bogotá D.C., Colombia;[3]Departmento de Geociencias, Universidad Nacional de Colombia, Bogotá, Colombia

Receiver Functions for 2016-2021 Show Slab Seismicity Most Abundant Where Low Velocity Zone Present at the Top of Slab, LAB of Slab Characterized by Variable Anisotropy

The young (<20 Myr old) Nazca plate currently subducting beneath western Colombia is a mosaic of former micro-plates separated by extinct spreading ridges. These extinct ridges have previously been shown to be associated with unusual sub-slab anisotropy (Idárraga-García et al. 2016) and a change between shallow angle and normal angle subduction (Vargas & Mann, 2013). These changes have led to the proposal that the traces of these ridges extend into the subducted slab as the Calderas and Malpelo Tears. Within the segment of subducted slab bounded by these tears slab seismicity appears extremely intense to the north and nearly non-existent to the south.

To investigate how these prior geophysical observations relate to structural features within the slab, we have used data for 3,022 >5.0 Mw teleseismic earthquakes occurring between 1 January 2016 and 31 December 2021 and located between 30° and 95° distance from the 24 seismometers of the Servicio Geológico Colombiano's Red Sismológica Nacional de Colombia permanent seismic network to calculate receiver functions (RFs; Ligorría & Ammon, 1999) in three different frequency bands. We assessed the resulting 200,000+ RFs to ensure they met a number of quality standards (e.g. highest amplitude in the initial peak on the radial component, lack of significant long period offsets, both radial and transverse components having >50% variance reduction), and found a total of 15,738 usable pairs of radial and transverse RFs.

RFs are sensitive to velocity changes across boundaries in the subsurface that are small compared to the dominant wavelength of the seismic data used to calculate the RFs. In the frequency domain, an RF is a Gaussian low-pass filter and increasing the "a"-parameter used to calculate an RF raises the frequencies contributing to the RF, lowering the dominant wavelength and making the RF more sensitive to more abrupt boundaries. We used "a"-parameters of 0.5, 1.0 and 2.5 to calculate our RFs, corresponding to peak frequencies of 0.24 Hz, 0.5 Hz, and 1.2 Hz, respectively. For S-wave velocities of 4.5 km/s, this translates to sensitivities to ~20 km, ~5-10 km, and ~1-5 km thick boundaries.

By first applying a moveout correction using the IASP91 velocity model to correct for differences in the angle of incidence between each RF and then averaging radial RFs at each station, we obtain estimates of the isotopic velocity structure beneath each station. We find good evidence for a low seismic velocity feature bounded by a negative (fast-over-slow material) RF arrival on top and a positive (slow-over-fast material) arrival on bottom where the Slab2 model (Hayes et al. 2018) predicts the top of the slab should lie. This feature is observed in the north where the slab is most seismically active. We also find broader, negative arrivals most prominent on the 0.24 Hz and 0.5 Hz RFs where the bottom of a ~10 Myr old, ~50 km thick slab should lie.

Calculation of the P-wave to S-wave velocity ratio (Vp/Vs) from earthquake sources within the slab shows that the low-velocity feature imaged by the RFs corresponds to the earthquake source region and that this region has unusually high Vp/Vs, requiring hydration and/or serpentinization. We interpret this to indicate the seismically active slab in the north is more hydrated than that in the south, and that the greater seismicity in the north is likely a result of the slab remaining hydrated to a greater depth in the north.

Examination of the negative arrival at the base of the slab shows that it is consistently most prominent on the 0.24 Hz and 0.5 Hz RFs and that this feature is not present at stations sampling the slab at >~400 km depth. This suggests that the feature represents the Lithosphere-Asthenosphere Boundary (LAB) of the slab. By averaging both the radial and transverse RFs for RFs coming from the down-dip, up-dip, northeast-strike, and southwest-strike directions for each station we find that the LAB exhibits an anisotropic pattern that cannot be explained purely by the dip of the slab. This indicates that there is a contrast in the direction of fast and slow anisotropy across the LAB. Quantitative analysis of this contrast is beyond the scope of this study, however we note that the contrast's character varies greatly between stations, indicating complex mantle flow possibly related to the tears.

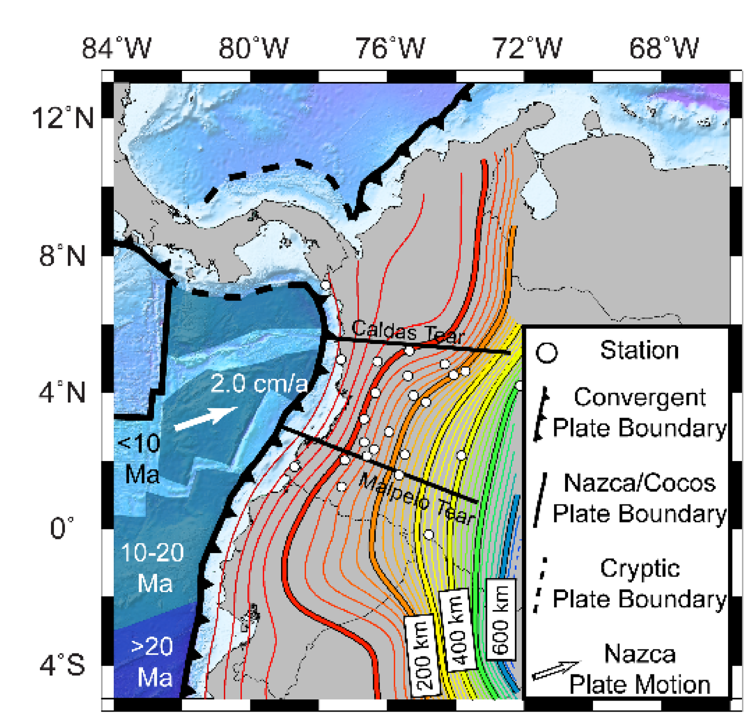

Tectonic Context & Relocated Seismicity

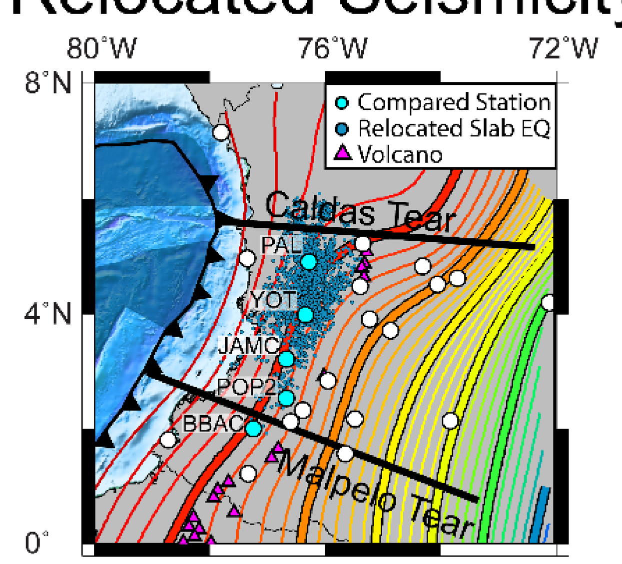

3°N to 5.5°N Region of High Slab Seismicity and Supra-Slab Seismicity

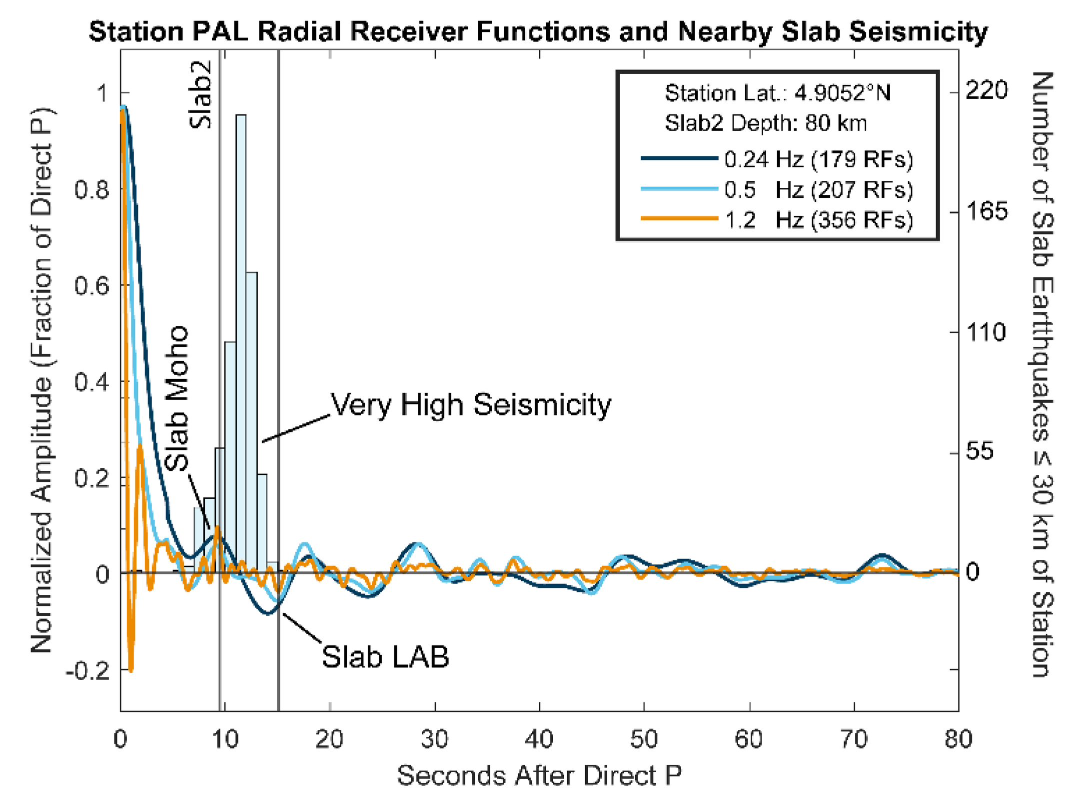

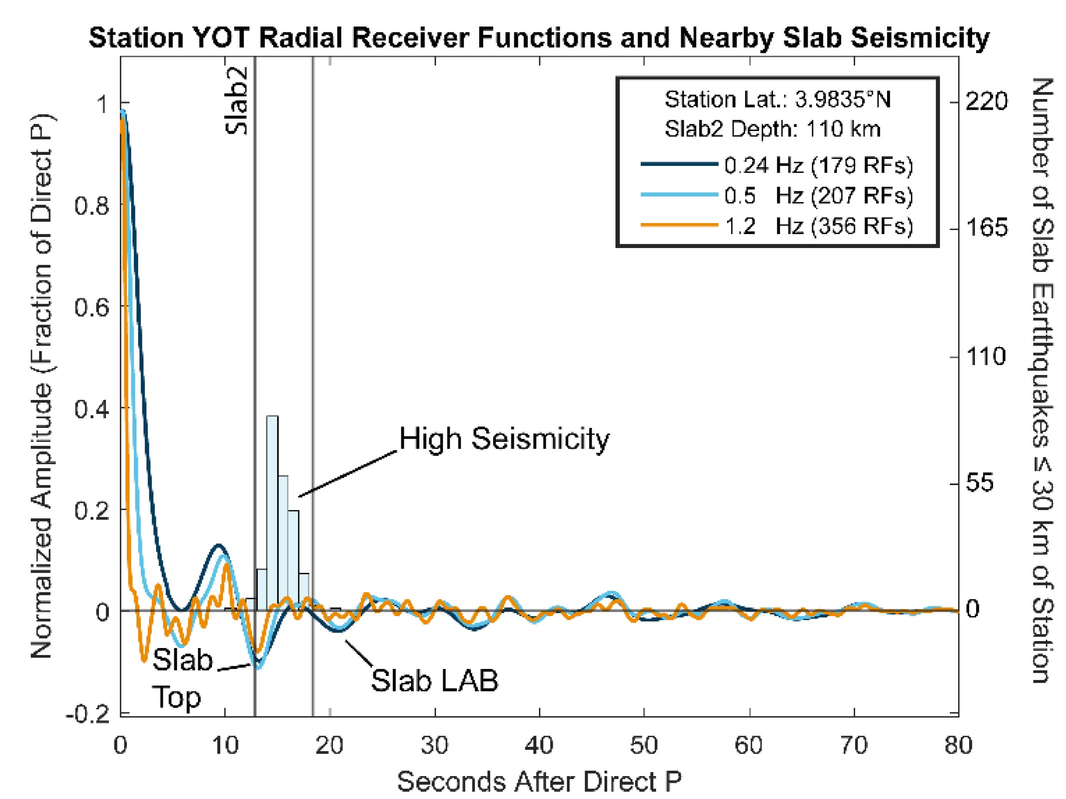

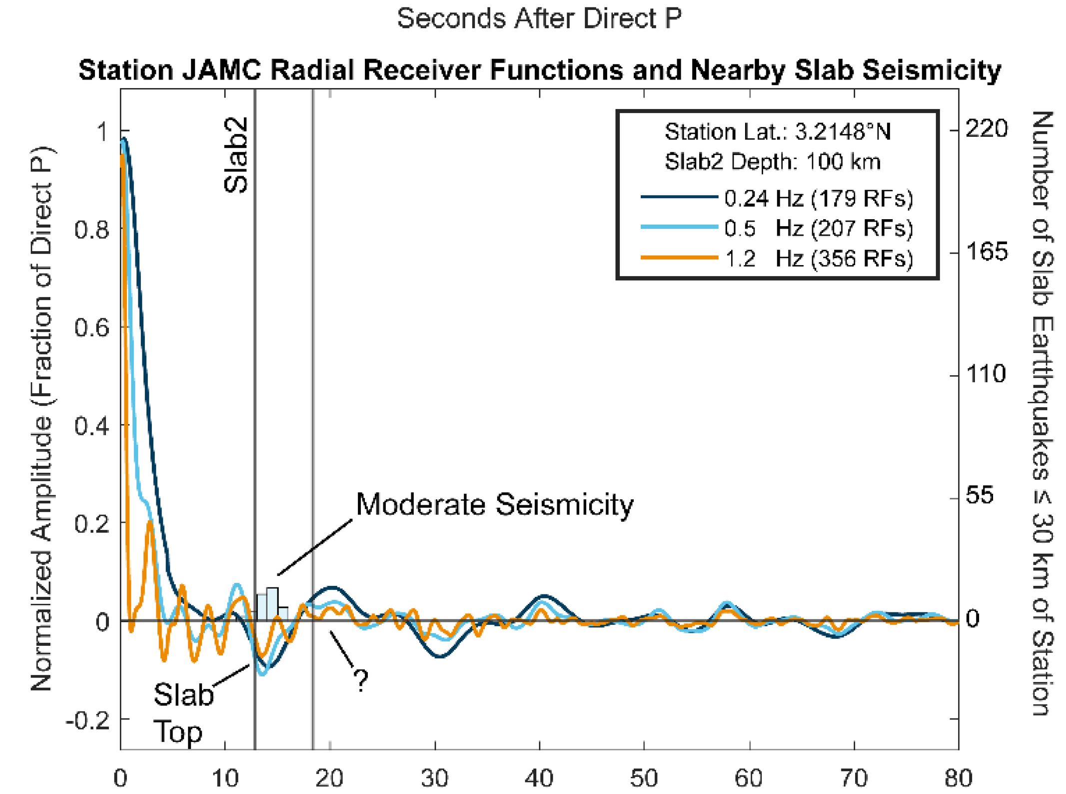

2°N to 3°N Region of Low Slab Seismicity

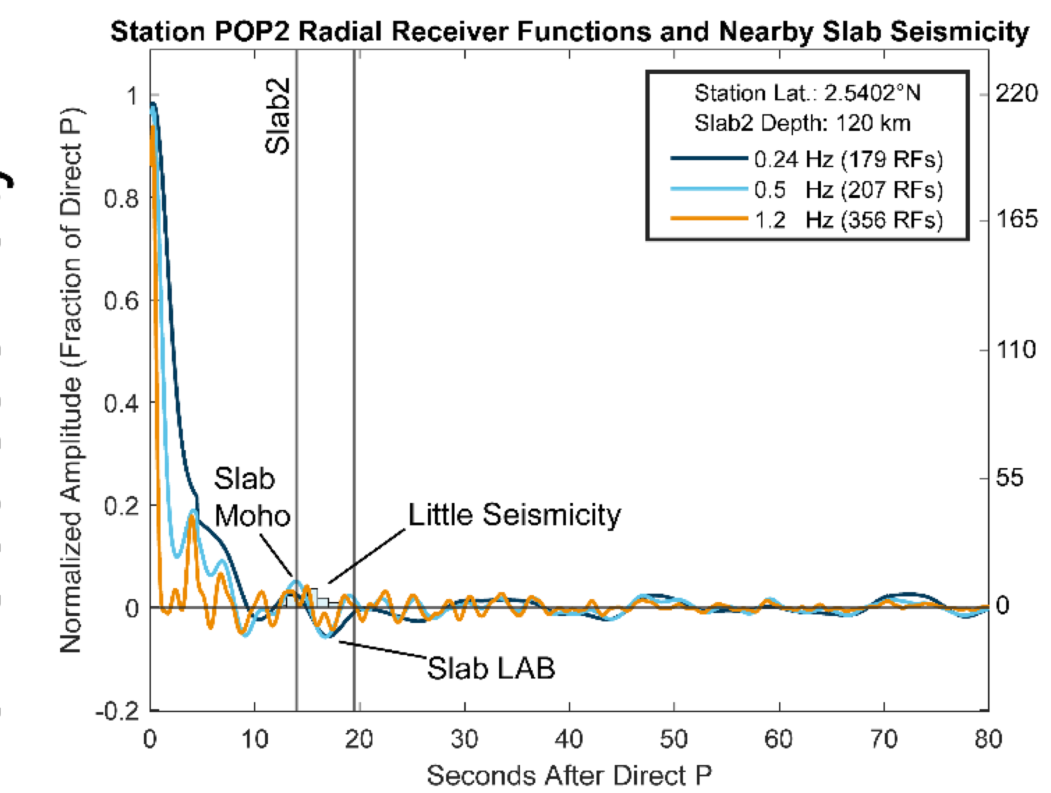

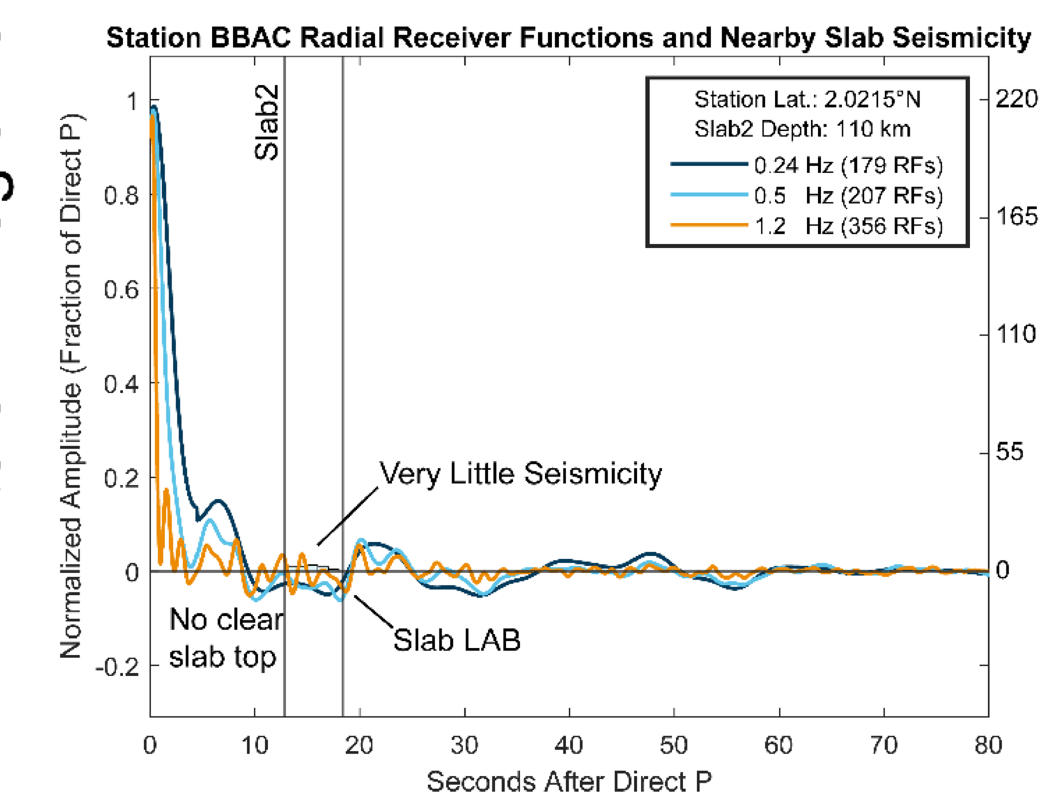

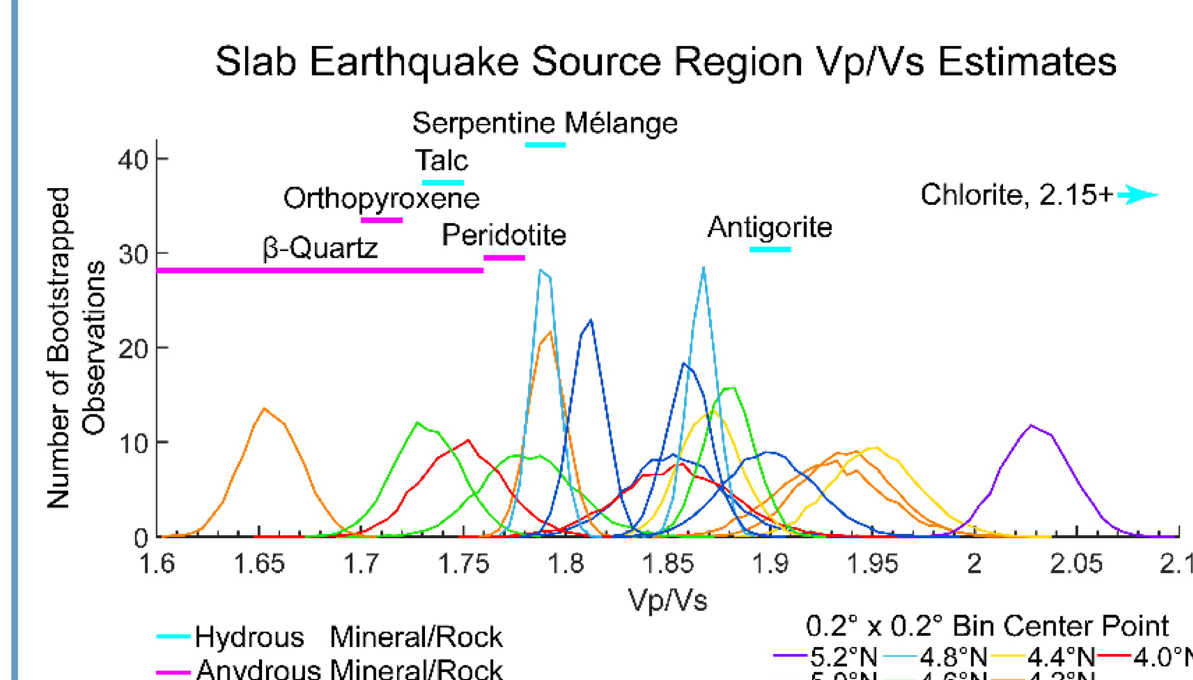

Example of Azimuthal, Anisotropy Induced Variations

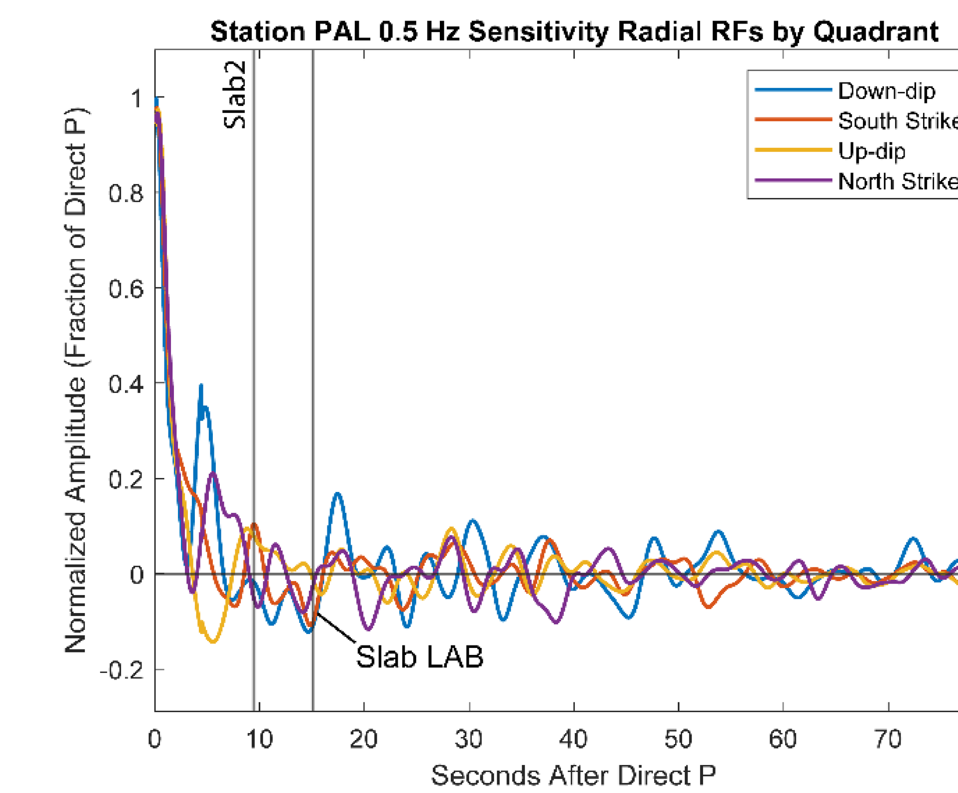

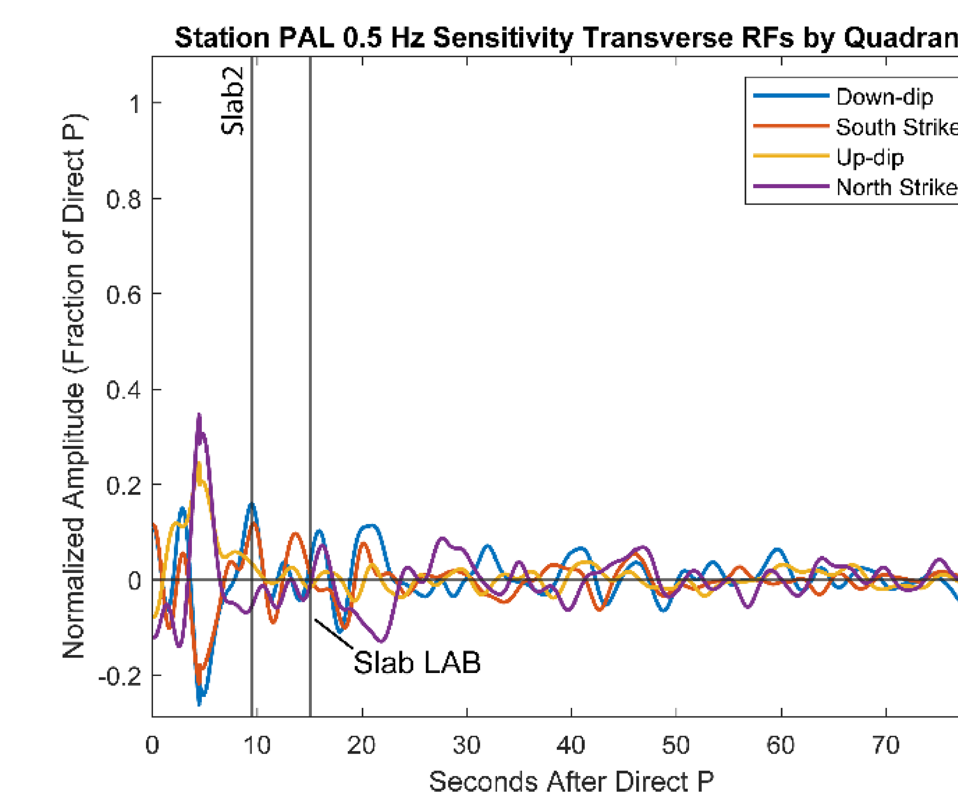

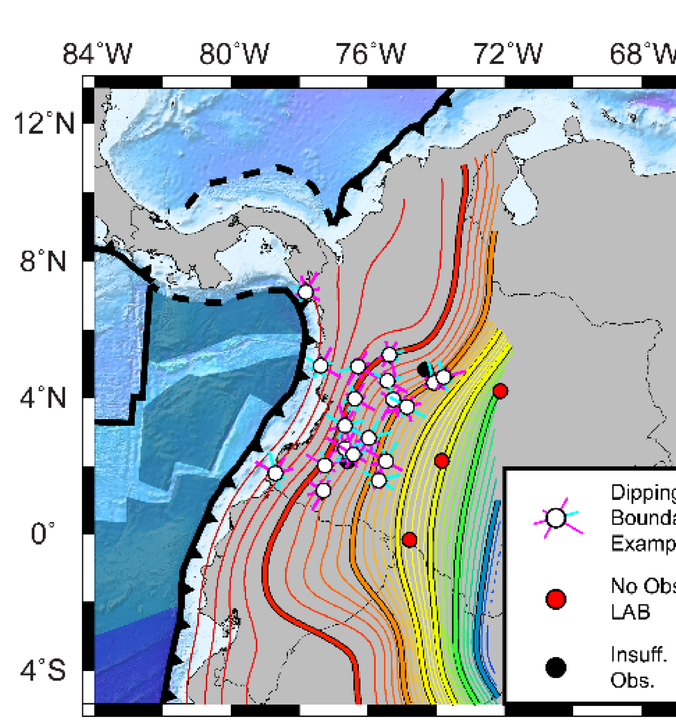

Map at left compares the observed amplitudes of the radial and transverse arrivals marking the slab LAB. Cyan indicates a positive arrival polarity and magenta indicates a negative arrival polarity. Rays in the down-dip (120°), up-dip (300°), northeast-strike (30°), and southwest-strike (210°) represent the radial component arrivals at each station; rays rotated 45° clockwise represent the same directions' arrivals on the transverse component. Dipping example is for a slab dipping southeast.

Acknowledgments: This work was supported by NSF grant EAR-2041631. We thank the RSNC staff for assistance regarding station metadata and information. We also thank the students and faculty at SLU's Earth and Atmospheric Sciences program for their support and help with this project.

References: Colombia tectonics: Gripp, A.E., Gordon, R.G., (2002). doi:10.1046/j.1365-246X.2002.01627.x. Idárraga-García, J., Kendall, J.-M., & Vargas, C.A. (2016). doi:10.1002/2016GC006323. Vargas, C.A., & Mann, P. (2013). doi:10.1785/0120120328. RF method: Ligorría, J.P., & Ammon, C.J. (1999). doi:10.1785/BSSA0890051395. Herrmann, R.B. (2013). doi:10.1785/0220110096. IASP91 velocity model: Kennett, B.L.N., & Engdahl, E.R., (1991). doi:10.17611/DP/9991809. Slab2: Hayes, G.P., Moore, G.L., Portner, D.E., Hearne, M., Flamme, H., Furtney, M., & Smoczyk, G.M. (2018). doi:10.1126/science.aat4723. Slab earthquakes: Bishop, B., Warren, L., Aravena, P., Cho, S., Soto-Cordero, L., Pedraza, P., Prieto, G., & Dionicio, V. (2021). doi:10.1002/essoar.10509166.1. Nazca age: Lonsdale, P. (2005). doi:10.1016/j.tecto.2005.05.011. Volcanoes: Global Volcanism Program (2023). doi:10.5479/si.GVP.VOTW5-2023.5.1. Vp/Vs values compiled from: Abers, G.A. & Hacker, B.R. (2016). doi:10.1002/2015GC006171. Codillo, E.A., Le Roux, V., & Marschall, H.R. (2018). doi:10.1038/s41467-018-05313-2. Hacker, B.R., & Abers, G.A. (2012). doi:10.1029/2012JB009187. Manthilake, G., Chantel, J., Guignot, N., & King, A. (2021). doi:10.3390/min11010070 Peng, Y., Mookherjee, M., Hermann, A., Manthilake, G., & Mainprice, D. (2022). doi:10.1016/j.gsf.2022.101381. Wang, D., Liu, T., Chen, T., Qi, X., & Li. B. (2019) doi:10.1029/2019GL082287.